

Intrinsic defects in photovoltaic perovskite variant Cs₂SnI₆

Zewen Xiao,^{1,2} Yuanyuan Zhou,³ Hideo Hosono,^{1,2} Toshio Kamiya^{1,2}

¹Materials and Structures Laboratory, Tokyo Institute of Technology, Yokohama 226-8503, Japan

²Materials Research Center for Element Strategy, Tokyo Institute of Technology, Yokohama 226-8503, Japan

³School of Engineering, Brown University, Providence, RI 02912, United States

ABSTRACT: Cs₂SnI₆ is a variant of perovskite materials and is expected as a lead-free air-stable photovoltaic material. In this letter, we report intrinsic defects in Cs₂SnI₆ using first-principles density functional theory calculations. It is revealed that iodine vacancy and tin interstitial are the dominant defects that are responsible for the intrinsic *n*-type conduction in Cs₂SnI₆. Tin vacancy has a very high formation energy (>3.6 eV) due to the strong covalency in the Sn–I bonds and is hardly generated for *p*-type doping. All the dominant defects in Cs₂SnI₆ have deep transition levels in the band gap. It is suggested that the formation of the deep defects can be suppressed significantly by employing an I-rich synthesis condition, which is inevitable for photovoltaic and other semiconductor applications.

Metal halide perovskites have been introduced as the “game-changer” materials in the novel solid-state solar cells.^{1–4} These perovskite compounds have the general chemical formula *ABX*₃ (*A* = Cs, CH₃NH₃, or CH₂NH=CH; *B* = Pb or Sn; *X* = I, Br or Cl), where the *A* cations sit in the cubic or pseudo-cubic network of corner-sharing *BX*₆ octahedra. Amongst these materials, tin (Sn) based perovskites *ASnX*₃ have attracted particular interest due to their nontoxicity.^{5–9} However, *ASnX*₃ are very sensitive to the ambient atmosphere (oxygen, moisture, etc.)^{7–12} and exploration for air-stable alternatives has become an urgent issue. Promisingly, Lee *et al.*¹³ recently reported that the Sn-based perovskite variant Cs₂SnI₆ exhibited high air-stability and their solar cells exhibit good efficiency as high as 8%. It is proposed that the superior stability of Cs₂SnI₆ to CsSnI₃ would be attributed to the +4 oxidation state of Sn in Cs₂SnI₆ based on a simple ionic model;¹³ on the other hand, density functional theory (DFT) calculations indicate that the real oxidation state of Sn in Cs₂SnI₆ is closer to +2, similar to CsSnI₃, which originates from the nominal formula Cs⁺₂Sn²⁺I₆^{4–}.¹⁴ In this view, the improved stability of Cs₂SnI₆ is attributed to the strong covalency of the Sn–I bonds in the isolated [SnI₆]^{2–} cluster.

It is known well that the typical Sn²⁺-based compounds, including SnO,¹⁵ SnS,^{16,17} and CsSnI₃,¹⁸ in general, intrinsically exhibit good *p*-type conductivity because V_{Sn} in these compounds are easily formed and act as shallow acceptors to produce mobile holes. On the other hand, Cs₂SnI₆ have not shown *p*-type conductivity unlike the other Sn²⁺-based compounds and have shown *n*-type conduction or insulating behavior depending on the synthetic routes. Lee *et al.*¹³ reported the native *n*-type conduction with electron density (*n*) of ~1×10¹⁴ cm⁻³ in polycrystalline Cs₂SnI₆ pellets annealed at 200 °C, while Zhang *et al.*¹⁹ observed very high resistivity in room temperature-processed Cs₂SnI₆. Therefore, in order to clarify the intrinsic nature of Cs₂SnI₆ and its origin, a

systematic theoretical study on the intrinsic defects is important, which will provide a guiding principle for tuning its properties for photovoltaic and other semiconductor applications.

Here, we studied the formation enthalpy (ΔH) of intrinsic defects in Cs₂SnI₆ by DFT calculations. It was clarified that I vacancy (V_I) and Sn interstitial (Sn_i) are mainly responsible for the intrinsic *n*-type conductivity in Cs₂SnI₆. V_{Sn}, which is usually a dominant *p*-type defect in Sn²⁺-based compounds, is hardly formed in Cs₂SnI₆ because of its high ΔH which is caused by the strong covalency of the Sn–I bonds in the isolated [SnI₆]^{2–} cluster. It was also clarified that intrinsic *p*-type conductivity is hardly be attained in pure Cs₂SnI₆ due to the absence of an effective acceptor with sufficiently low ΔH and a shallow transition level. The origin of deep transition levels of the dominant defects in Cs₂SnI₆ will be discussed.

Defect calculations were performed in the framework of DFT using the projector-augmented wave (PAW) method as implemented in the VASP code.²⁰ Cs (5s)(5p)(6s), Sn (5s)(5p), and I (5s)(5p) orbitals are treated as valence states in the PAW potentials. The cutoff energy for the basis set was set to 275.4 eV. A 72-atoms supercell (2×2×2 primitive cells) was used to model the intrinsic defects. Atomic positions were relaxed until all the forces on the atoms were less than 0.05 eV/Å, employing a Γ -centered 3×3×3 *k*-mesh and the Perdew–Burke–Ernzerhof (PBE96)²¹ generalized gradient approximation (GGA) functionals. The total energies were calculated with a Γ -centered 2×2×2 *k*-mesh using the Heyd–Scuseria–Ernzerhof (HSE06)²² hybrid functional with 34% of exact nonlocal exact exchange, which was adjusted to reproduce the experimental band gap of 1.26 eV as reported in Ref. 13.

ΔH of a defect (*D*) in a charge state *q* was calculated through the following equation²³

$$\Delta H_{D,q}(E_F, \mu) = E_{D,q} - E_H - \sum n_\alpha \mu_\alpha + q(E_F + E_V + \Delta V), \quad (1)$$

where $E_{D,q}$ is the total energies of the supercell with the defect *D* in the charge state *q*, and E_H that of the perfect host supercell. n_α indicates the number of α atoms added ($n_\alpha > 0$) or removed ($n_\alpha < 0$), and μ_α is the chemical potential of an α atom with respect to that of an elemental phase (μ_α^{el}) by $\mu_\alpha = \mu_\alpha^{\text{el}} + \Delta\mu_\alpha$. E_F is the Fermi level relative to the valence band maximum (VBM, E_V), which was corrected by ΔV through electrostatic potential alignment.²³ For charged defects, the image charge correction was also applied to eliminate the supercell finite-size effects.²⁴

μ_α varies depending on the experimental condition during growth or annealing. First, to stabilize the Cs₂SnI₆ phase, the following thermodynamic equation must be satisfied

$$2\Delta\mu_{\text{Cs}} + \Delta\mu_{\text{Sn}} + 6\Delta\mu_{\text{I}} = \Delta H(\text{Cs}_2\text{SnI}_6) = -10.49 \text{ eV}, \quad (2)$$

where $\Delta H(\text{Cs}_2\text{SnI}_6)$ is ΔH of Cs_2SnI_6 referred to the elemental Cs, Sn, and I. To avoid the coexistence of the Cs, the Sn, and the I elemental phases, the additional conditions, $\Delta\mu_{\text{Cs}} < 0$, $\Delta\mu_{\text{Sn}} < 0$, and $\Delta\mu_{\text{I}} < 0$, are required. To exclude the secondary phases CsI (cubic, space group $Pm\bar{3}m$),²⁵ SnI_2 (monoclinic, space group $C2/m$),²⁶ SnI_4 (cubic, space group $Pa\bar{3}$),²⁷ and CsSnI_3 (cubic, space group $Pm\bar{3}m$),⁹ the following constraints must be satisfied as well.

$$\Delta\mu_{\text{Cs}} + \Delta\mu_{\text{I}} < \Delta H(\text{CsI}) = -3.80 \text{ eV}, \quad (3)$$

$$\Delta\mu_{\text{Sn}} + 2\Delta\mu_{\text{I}} < \Delta H(\text{SnI}_2) = -1.69 \text{ eV}, \quad (4)$$

$$\Delta\mu_{\text{Sn}} + 4\Delta\mu_{\text{I}} < \Delta H(\text{SnI}_4) = -2.40 \text{ eV}, \quad (5)$$

$$\Delta\mu_{\text{Cs}} + \Delta\mu_{\text{Sn}} + 3\Delta\mu_{\text{I}} < \Delta H(\text{CsSnI}_3) = -5.77 \text{ eV}. \quad (6)$$

With all these equations satisfied, $\Delta\mu_{\text{Sn}}$ and $\Delta\mu_{\text{I}}$ (and, thus, $\Delta\mu_{\text{Cs}}$ determined from Eq 2) are limited to a narrow region as shown by the yellow region defined by the A–B–C–D points in Figure 1. The narrow shape indicates that the growth or annealing conditions should be carefully controlled to produce the single-phase Cs_2SnI_6 , similar to the cases of CsSnI_3 ¹⁸ and MAPbI_3 .²⁸

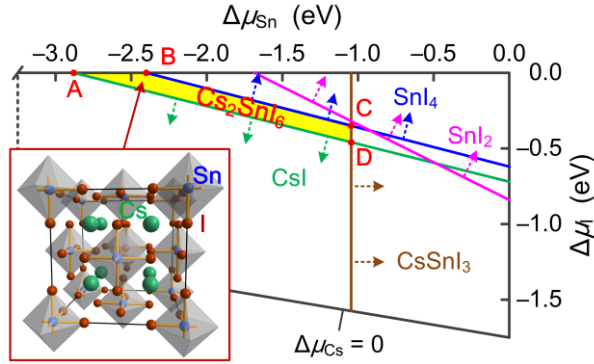


Figure 1. $(\Delta\mu_{\text{Sn}}, \Delta\mu_{\text{I}})$ chemical potential – phase map. The yellow region A–B–C–D shows the region where Cs_2SnI_6 is stabilized against possible competitive phases including Cs, Sn, I, CsI, SnI_2 , SnI_4 , and CsSnI_3 . The inset on left shows the crystal structure of Cs_2SnI_6 .

From the $\Delta H_{D,q}$, the defect transition level $\varepsilon(q/q')$ between two charge states q and q' is obtained as the E_{F} where $\Delta H_{D,q}(E_{\text{F}}, q) = \Delta H_{D,q}(E_{\text{F}}, q')$. The equilibrium Fermi level ($E_{\text{F,e}}$) and carrier concentration at room temperature were determined by solving semiconductor statistic equations self-consistently so as to satisfy the charge neutrality.^{16,29}

We have considered intrinsic point defects in Cs_2SnI_6 including three vacancies (V_{Cs} , V_{Sn} , V_{I}), three interstitials (Cs_{I} , Sn_{I} , I_{I}), two cation substitutions (Cs_{Sn} , Sn_{Cs}), and four antisites (Cs_{I} , Sn_{I} , I_{Cs} , I_{Sn}). Two representative chemical potential conditions in Figure 1 are chosen for discussion; $(\Delta\mu_{\text{Cs}}, \Delta\mu_{\text{I}})$ at A (I-rich condition) and D (I-poor) points. The calculated $\Delta H_{D,q}$ under the I-rich and I-poor conditions are plotted as a function of E_{F} in Figures 2a and 2b, respectively. The calculated $\varepsilon(q/q')$ are plotted relative to the conduction band minimum (CBM) and valence band maximum (VBM) in Figure 3. Out of the twelve intrinsic defects, four (V_{I} , Sn_{I} , Cs_{I} and V_{Cs}) have a sufficiently small ΔH (e.g., < 1.0 eV) to influence the electrical properties. Among them, V_{I} has the lowest ΔH (≤ 0.74 eV and ≤ 0.28 eV under I-rich and I-poor conditions, respectively) and acts as a deep donor with $\varepsilon(0/+1) = 0.74$ eV above VBM (i.e., 0.52 eV below the conduction band edge, CBM), which is mainly responsible for the n -type condition of Cs_2SnI_6 . Under the I-poor condition, Sn_{I} has a small ΔH (≤ 1.18 eV) and a shallower transition $\varepsilon(0/+1)$ at 0.11 eV below the CBM. Therefore, Sn_{I} as well as V_{I} are also dominant donors for n -type conduction. Cs_{I} is of a low ΔH but stabilized in the neutral charge state at high

E_{F} (i.e. n -type conditions); therefore, it does not contribute to the n -type conduction. Only Sn_{I} is a shallow donor in Cs_2SnI_6 with the $\varepsilon(0/+2)$ above the CBM, as seen in Figures 2b and 3. However, because of its relatively high ΔH , Sn_{I} has limited contribution to the n -type conductivity even under the I-poor condition. On the other hand, under the I-rich condition, V_{Cs} has a low ΔH (≤ 1.37 eV) and can act as a deep acceptor, but at E_{F} only above 0.51 eV from the VBM and the hole density produced is too low to compensate the electrons released by V_{I} .

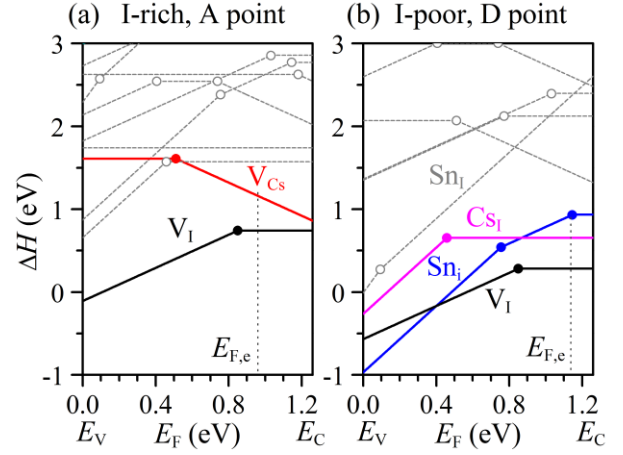


Figure 2. Calculated ΔH of intrinsic defects in Cs_2SnI_6 as a function of E_{F} at the chemical potential points in Figure 1, (a) A (I-rich) and (b) D (I-poor). Defects with much high ΔH values are shown by dashed lines.

The other intrinsic defects with prohibitively high ΔH are displayed by gray dashed lines in Figure 2. It should be noted that V_{Sn} in Cs_2SnI_6 has high ΔH values under all the chemical potentials and is as large as 3.63 eV even under the Sn-poor condition (A point), as seen in Table 1. This is strikingly different from the cases of the typical Sn^{2+} -based semiconductors such as SnO ,¹⁵ SnS ,^{16,17} and CsSnI_3 ,¹⁸ in which the ΔH values of V_{Sn} (at the VBM) are usually very small under the Sn-poor condition (i.e., 1.3 eV at E_{V} for SnO ,¹⁵ 0.8 eV for SnS ,^{16,17} and 0.3 eV for CsSnI_3 ¹⁸). As we previously reported, the Sn–I bonds in Cs_2SnI_6 exhibit a strong covalency (2.40 eV/bond) due to the much shortened Sn–I length in the isolated $[\text{SnI}_6]^{2-}$ octahedra.¹⁴ Sn atoms are tightly encased in the $[\text{I}_6]$ octahedra and hardly removed by thermal fluctuation, which explains the unusually high ΔH of V_{Sn} in Cs_2SnI_6 . Due to the same reason, the substitutions of Sn by Cs and I (i.e., Cs_{Sn} and I_{Sn}) have similarly high ΔH values. We have proposed that the +2 valence state of Sn in Cs_2SnI_6 is stabilized by the strong covalency of the Sn–I bonds.¹⁴ Here, the high ΔH of the Sn-site-related defects further support the stabilized +2 valence state of Sn in Cs_2SnI_6 .

Since it is found any intrinsic defect does not work as an effective p -type source from the I-rich to I-poor conditions, as shown above, it would be difficult to achieve intrinsic p -type conduction in pure Cs_2SnI_6 . Instead, Cs_2SnI_6 intrinsically exhibits n -type conduction due to the easy formation of V_{I} and Sn_{I} donors. For quantitative analysis, the equilibrium E_{F} ($E_{\text{F,e}}$) at room temperature was calculated by considering all the $\Delta H_{D,q}$ values and the semiconductor statistics, giving $E_{\text{F,e}} - E_{\text{V}} = 0.96$ eV (i.e. $E_{\text{C}} - E_{\text{F,e}} = 0.30$ eV) for the I-rich limit at A point (Figure 2a) and $E_{\text{F,e}} - E_{\text{V}} = 1.14$ eV (i.e. $E_{\text{C}} - E_{\text{F,e}} = 0.12$ eV) for the I-rich limit at A point (Figure 2b), corresponding to a low n of $\sim 10^{12} \text{ cm}^{-3}$ (such value is not easily determined by a Hall effect measurements) and a much higher value of $\sim 10^{16} \text{ cm}^{-3}$, respectively. These theoretical results seem to explain the experimental results reported to date; i.e., the

electrical properties of Cs_2SnI_6 ranging from insulating¹⁹ to low-density n -type conduction ($n \sim 1 \times 10^{14} \text{ cm}^{-3}$).¹³

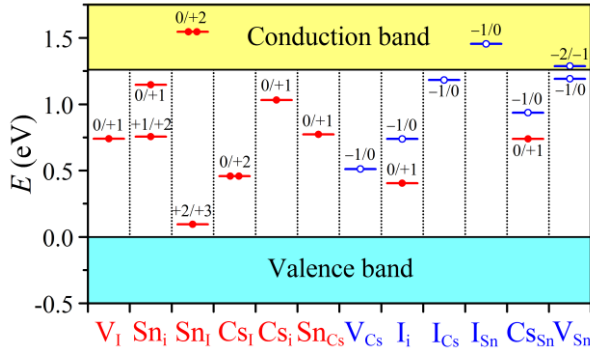


Figure 3. Calculated transition energy levels $\varepsilon(q/q')$ for intrinsic defects in Cs_2SnI_6 . Donor and acceptor defect levels are denoted by red and blue bars, respectively. The solid and open circles at the transition levels show the number of electrons and holes that can be released during the transition of the defect charge state.

Table 1. Formation enthalpies (in eV) of twelve intrinsic defects in Cs_2SnI_6 at the chemical potential points A, B, C, and D shown in Figure 1.

	V_{Cs}	V_{Sn}	V_{I}	Cs_i	Sn_i	I_i	Cs_{Sn}	Sn_{Cs}	Cs_i	Sn_i	I_{Cs}	I_{Sn}
A	1.61	3.63	0.74	2.86	2.77	2.54	3.74	3.50	1.57	5.47	2.62	1.74
B	1.37	4.11	0.74	3.10	2.28	2.54	4.46	2.78	1.81	4.98	2.38	2.23
C	1.71	5.47	0.40	2.76	0.93	2.88	5.48	1.76	1.14	3.29	3.06	3.92
D	2.07	5.47	0.28	2.40	0.93	3.00	5.12	2.12	0.65	3.17	3.54	4.04

The $\varepsilon(q/q')$ of the dominant defects are important in particular for solar cells because $\varepsilon(q/q')$ in the band gap indicates that they work as an electron trap, hole trap, and/or a recombination center, which deteriorate the device performances. The dominant defects V_{Pb} in MAPbI_3 ²⁸ and V_{Sn} in CsSnI_3 ¹⁸ have transition levels deeper than their VBMs and are inert. Also in CuInSe_2 , the dominant defect V_{Cu} has an $\varepsilon(-1/0)$ at only 0.03 eV above the VBM.³¹ The very shallow V_{Cu} results in good p -type good conduction but does not deteriorate the photovoltaic performance. In contrast, in Cs_2SnI_6 , all the dominant defects (Cs_i , Sn_i , V_{I} , V_{Cs} as shown by the solid lines in Figure 2) have $\varepsilon(q/q')$ in the band gap, as seen in Figure 3, which would more or less hinder photovoltaic performances through short diffusion/drift length and fast recombination of photo-generated carriers, in particular when processed under the I-poor condition. These deep defects can, however, be significantly avoided by using I-rich conditions, which is located at the phase boundary between Cs_2SnI_6 and elemental I (e.g. the B point as shown in Figure 2a), because their ΔH are considerably increased as seen in Table 1.

The defect properties as well as electronic structure of a material can qualitatively understood well based on the molecular orbital theory.^{28,30,32} Here we provides a simplified interpretation for the origin of the deep nature of the intrinsic defects in Cs_2SnI_6 in comparison with representative Sn^{2+} -based compounds such as SnO and CsSnI_3 , by focusing on cation and anion vacancies, which generally have low ΔH and play important role on electrical properties of these compounds. As depicted in Figure 4a, the VBM of SnO consists of the antibonding state of $\text{Sn } 5s$ and $\text{O } 2p$ orbitals.³³ Here, we should consider that, without the $\text{Sn } 5s$ orbitals, the VBM should be formed by $\text{O } 2p$ - $\text{O } 2p$ antibonding states.²⁸ When a cation vacancy V_{Sn} is formed, the defect level would be close to the $\text{O } 2p$ - $\text{O } 2p$ antibonding levels because this defect has a strong nature of the $\text{O } 2p$ - $\text{O } 2p$ antibonding states that is non-bonding to a Sn. Since the VBM is pushed up to a

higher level than the $\text{O } 2p$ - $\text{O } 2p$ antibonding states due to the strong $\text{Sn } 5s$ - $\text{O } 2p$ antibonding interaction. In this simple picture, V_{Sn} should lie at a lower energy than VBM, but formation of a vacancy usually induces structural relaxation, stabilizes a defect state, and pushes down the defect energy for a donor state, as reported in V_{O} in ZnO .³⁴ For V_{Sn} in SnO , the formation of the acceptor V_{Sn} induces structural relaxation and its energy level is relaxed with respect to a hole and pushes up the V_{Sn} state, resulting in the V_{Sn} level slightly above the VBM, which is responsible for the p -type conduction. On the other hand, the CBM consists of antibonding $\text{Sn } 5p$ - $\text{O } 2p$ states and is close to the $\text{Sn } 5p$ level due to the ionic character of SnO . For an oxygen vacancy V_{O} , the defect state is composed of the Sn non-bonding state, which lies close to the CBM,³² resulting in the shallow nature of V_{O} . Figure 2b schematically illustrates the formation of the CBM, VBM, V_{Sn} , and V_{I} in CsSnI_3 . Since the Cs cation does not contribute to the electronic structure around the band gap, the electronic structure of CsSnI_3 is similar to that of SnO if O is replaced with I. As a result, V_{Sn} and V_{I} in CsSnI_3 act as a shallow acceptor and a shallow donor, respectively.¹⁸ In contrast, Cs_2SnI_6 has a strikingly different electronic structure as reported in a previous paper¹⁴ and is schematically illustrated in Figure 4c. Because of the shortened Sn-I length (2.85 Å) in Cs_2SnI_6 compared with that of CsSnI_3 (3.10 Å), the covalent couplings between $\text{Sn } 5s$ and $\text{I } 5p$ and between $\text{Sn } 5p$ and $\text{I } 5p$ are much stronger in Cs_2SnI_6 than those in CsSnI_3 . The resulting $\text{Sn } 5s$ - $\text{I } 5p$ and the $\text{Sn } 5p$ - $\text{I } 5p$ antibonding states in Cs_2SnI_6 are located at much higher energies than those in CsSnI_3 , where the former forms unoccupied CBM states. The $\text{Sn } 5s$ level is deep similar to SnO and CsSnI_3 and fully occupied, resulting in the +2 oxidation state of Sn. The $\text{Sn } 5p$ - $\text{I } 5p$ antibonding states, which forms CBM in CsSnI_3 , forms an upper conduction band in Cs_2SnI_6 because the $\text{Sn } 5s$ - $\text{I } 5p$ antibonding unoccupied states are located at the lower energy. Consequently, the VBM consists of the $\text{I } 5p$ - $\text{I } 5p$ antibonding states. When V_{Sn} is formed, the defect state created by V_{Sn} is formed by the $\text{I } 5p$ - $\text{I } 5p$ antibonding states that are non-bonding to an Sn and its level is relaxed to a higher energy similar to the CsSnI_3 case but below the CBM for the Cs_2SnI_6 case due to the very high CBM level as explained above. On the other hand, when a V_{I} is formed, the defect state generated by V_{I} consists mainly of the $\text{Sn } 5s$ that is non-bonding to an I but bonded to the other remaining I; consequently, the V_{I} level is located around CBM in the band gap. Form these results, we conclude that the deep defect transitions in Cs_2SnI_6 originate from the strong covalency of Sn-I bonds, similar to the typical covalent compounds such as GaAs .²³

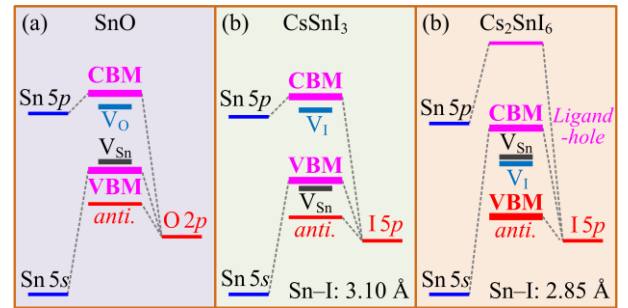


Figure 4. Simplified energy diagrams depicting the formation of VBM, CBM, and donor-/acceptor-like defects in (a) $\text{Sn}^{2+}\text{O}_2^-$, (b) $\text{Cs}^+\text{Sn}^{2+}\text{I}_3^-$, and (c) $\text{Cs}^+_2\text{Sn}^{2+}\text{I}_6^{4-}$.

In summary, we have investigated the formation energies of intrinsic defects in the Cs_2SnI_6 perovskite variant. The dominant defects are donor V_{I} and Sn_i , giving the calculated electron densities of 10^{12} - 10^{16} cm^{-3} . Unlike other Sn^{2+} -based p -type semiconductor such as SnO , SnS and CsSnI_3 , the V_{Sn} in Cs_2SnI_6 has a very high $\Delta H > 3.6 \text{ eV}$ and are hardly formed, primarily because

of the strong Sn–I covalent bonds in the functional group-like $[\text{SnI}_6]^{2-}$ isolated cluster. Also because of the strong covalency, the energy levels of the dominant defects are deep in the band gap and would work as recombination centers in photovoltaic applications. On the other hand, their formations would be practically suppressed by employing an I-rich synthesis condition where their densities are negligibly small due to the high ΔH . These results explain the reported experimental results and provide a clue to better understanding the unusual defect physics in *p*-block metal-based compounds.

This work was conducted under Tokodai Institute for Element Strategy (TIES) funded by MEXT Elements Strategy Initiative to Form Core Research Center. Y.Z. thanks Prof. Nitin P. Padture and U.S. National Science Foundation (DMR-1305913) for the support.

REFERENCES

- 1 M. A. Green, T. Bein, *Nat. Mater.* **14**, 559 (2015).
- 2 W. S. Yang, J. H. Noh, N. J. Jeon, Y. C. Kim, S. Ryu, J. Seo, and S. I. Seok, *Science* doi: 10.1126/science.aaa9272 (2015).
- 3 Y. Zhou, M. Yang, W. Wu, A. L. Vasiliev, K. Zhu, N. P. Padture, *J. Mater. Chem. A* **3**, 8178 (2015)
- 4 Y. Kutes, L. Ye, Y. Zhou, S. Pang, B. D. Huey and N. P. Padture, *J. Phys. Chem. Lett.* **5**, 3335 (2014)
- 5 F. Hao, C. C. Stoumpos, D. H. Cao, R. P. H. Chang, and M. G. Kanatzidis, *Nat. Photonics* **8**, 489 (2014).
- 6 J. Feng and B. Xiao, *J. Phys. Chem. C* **118**, 19655 (2014).
- 7 N. K. Noel, S. D. Stranks, A. Abate, C. Wehrenfennig, S. Guarnera, A.-A. Haghighirad, A. Sadhanala, G. E. Eperon, S. K. Pathak, M. B. Johnston, A. Petrozza, L. M. Herz, and H. J. Snaith, *Energy Environ. Sci.* **7**, 3061 (2014).
- 8 I. Chung, B. Lee, J. He, R. P. H. Chang, and M. G. Kanatzidis, *Nature* **485**, 486 (2012).
- 9 I. Chung, J. H. Song, J. Im, J. Androulakis, C. D. Malliakas, H. Li, A. J. Freeman, J. T. Kenney, and M. G. Kanatzidis, *J. Am. Chem. Soc.* **134**, 8579 (2012).
- 10 Z. Chen, J. J. Wang, Y. Ren, C. Yu, and K. Shum, *Appl. Phys. Lett.* **101**, 093901 (2012).
- 11 Y. Zhou, H. F. Garces, B. S. Senturk, A. L. Ortiz, and N. P. Padture, *Mater. Lett.* **110**, 127 (2013).
- 12 E. Lora da Silva, J. M. Skelton, S. C. Parker and A. Walsh, *Phys. Rev. B* **91**, 144107 (2015).
- 13 B. Lee, C. C. Stoumpos, N. Zhou, F. Hao, C. Malliakas, C.-Y. Yeh, T. J. Marks, M. G. Kanatzidis, and R. P. H. Chang, *J. Am. Chem. Soc.* **136**, 15379 (2014).
- 14 Z. Xiao, H. Lei, X. Zhang, Y. Zhou, H. Hosono, and T. Kamiya, *Bull. Chem. Soc. Jpn.* doi:10.1246/bcsj.20150110 (2015).
- 15 A. Togo, F. Oba, I. Tanaka, and K. Tatsumi, *Phys. Rev. B* **74**, 195128 (2006).
- 16 Z. Xiao, F.-Y. Ran, H. Hosono, and T. Kamiya, *Appl. Phys. Lett.* **106**, 152103 (2015).
- 17 F.-Y. Ran, Z. Xiao, Y. Toda, H. Hiramatsu, H. Hosono, and T. Kamiya, *Sci. Rep.* **5**, 10428 (2015).
- 18 P. Xu, S. Chen, H.-J. Xiang, X.-G. Gong, and S.-H. Wei, *Chem. Mater.* **26**, 6068 (2014).
- 19 J. Zhang, C. Yu, L. Wang, Y. Li, Y. Ren, and K. Shum, *Sci. Rep.* **4**, 6954 (2014).
- 20 G. Kresse and J. Furthmüller, *Phys. Rev. B* **54**, 11169 (1996).
- 21 J. P. Perdew, K. Burke, and M. Ernzerhof, *Phys. Rev. Lett.* **77**, 3865 (1996).
- 22 J. Heyd, G. E. Scuseria, and M. Ernzerhof, *J. Chem. Phys.* **118**, 8207 (2003).
- 23 C. G. Van de Walle and J. Neugebauer, *J. Appl. Phys.* **95**, 3851 (2004).
- 24 S. Lany and A. Zunger, *Phys. Rev. B* **78**, 235104 (2008).
- 25 A. Smakula and J. Kalnajs, *Phys. Rev.* **99**, 1737 (1955).
- 26 R.A. Howie, W. Moser, and I. C. Trevena, *Acta Crystallogr.* **B28**, 2965 (1972).
- 27 R. G. Dickinson, *J. Am. Chem. Soc.* **45**, 958 (1923).
- 28 W.-J. Yin, T. Shi, and Y. Yan, *Appl. Phys. Lett.* **104**, 063903 (2014).
- 29 D. B. Laks, C. G. Van de Walle, G. F. Neumark, P. E. Blöchl, and S. T. Pantelides, *Phys. Rev. B* **45**, 10965 (1992).
- 30 W.-J. Yin, S.-H. Wei, M. M. Al-Jassim, and Y. Yan, *Appl. Phys. Lett.* **99**, (2011).
- 31 S. B. Zhang, S.-H. Wei, A. Zunger, and H. Katayama-Yoshida, *Phys. Rev. B* **57**, 9642 (1998).
- 32 W.-J. Yin, T. Shi, and Y. Yan, *J. Phys. Chem. C* **119**, 5253 (2015).
- 33 M. Liao, Z. Xiao, F.-Y. Ran, H. Kumomi, T. Kamiya, and H. Hosono, *ECS J. Solid State Sci. Technol.* **4**, Q26 (2015).
- 34 F. Oba, A. Togo, I. Tanaka, J. Paier, and G. Kresse, *Phys. Rev. B - Condens. Matter Mater. Phys.* **77**, (2008).